Applied Physics Letters

RESEARCH ARTICLE | JUNE 17 2024

Calculation model of rectangular-like Herriott cell based on folded-optics method

Qingyuan Tian ; Hongpeng Wu ; Ruyue Cui; Yongyong Hu ; Yan Xue; Gang Wang ; Jiapeng Wang ; Yong Wang; Xiaoli Liu; Frank K. Tittel; Lei Dong

Appl. Phys. Lett. 124, 251102 (2024)
https://doi.org/10.1063/5.0206483

Applied Physics Letters ARTICLE pubs.aip.org/aip/apl

Calculation model of rectangular-like Herriott cell based on folded-optics method

Cite as: Appl. Phys. Lett. **124**, 251102 (2024); doi: 10.1063/5.0206483
Submitted: 2 March 2024 · Accepted: 15 May 2024 ·
Published Online: 17 June 2024

Qingyuan Tian,[1,2] Hongpeng Wu,[1,2] Ruyue Cui,[1,2] Yongyong Hu,[1,2] Yan Xue,[1,2] Gang Wang,[1,2] Jiapeng Wang,[1,2] Yong Wang,[1,2] Xiaoli Liu,[1,2] Frank K. Tittel,[3] and Lei Dong[1,2,a)]

AFFILIATIONS

[1]State Key Laboratory of Quantum Optics and Quantum Optics Devices, Institute of Laser Spectroscopy, Shanxi University, Taiyuan 030006, China
[2]Collaborative Innovation Center of Extreme Optics, Shanxi University, Taiyuan 030006, China
[3]Department of Electrical and Computer Engineering, Rice University, 6100 Main Street, Houston, Texas 77005, USA

[a)]**Author to whom correspondence should be addressed:** donglei@sxu.edu.cn

ABSTRACT

We present a calculation model for rectangular-like Herriott cells (RLHCs), in which a long cylindrical traditional Herriott cell (HC) is transformed into a rectangular-like configuration by introducing two highly reflective plane mirrors. The position formula for two spheric mirrors and two plane mirrors is provided to precisely define the RLHC. The folding effects of RLHCs with 1–8-times folding are evaluated in terms of the cell length, the cell volume, and the total number of reflections. The proposed folded-optics method significantly enhances the utilization efficiency of the mirror surfaces, resulting in a reduction of both physical length and volume when compared to a traditional HC. Importantly, this reduction is achieved while maintaining the same optical path length, and all of these advantages come at a low cost.

Multi-pass cell (MPC), comprised of several highly reflective mirrors, is a vital optical detection module meticulously designed to attain significantly extended optical path lengths within a confined volume. The design methodology of MPC has been a focal point in the field of absorption spectroscopy research[1–5] due to the fact that enhancing the effective optical path stands as the most direct and straightforward approach to improving detection sensitivity, aligning with the fundamental principles elucidated in the Beer–Lambert law. In recent years, various types of MPCs have been developed, with the majority constructed using cylindrical mirrors, specially designed mirrors, or other mirrors with complex reflective surfaces.[6–8] However, the production of aspherical surfaces is so intricate that attaining an ideal mirror with precise surfaces becomes challenging. In contrast, spherical surfaces only require grinding and polishing, which are well-established and widely used techniques in mirror manufacturing.[9] In addition, in recent years, there have been various studies on reducing cell size by introducing multiple mirrors,[10–12] but the spot overlap in these multi-pass cells and the volume are still large.

Herriott cell (HC), a quintessential example of spherical mirror MPCs, continues to be extensively utilized[13,14] owing to its four principal advantages: (1) The HC is comprised of commercially available spherical mirrors, facilitating straightforward construction; (2) the small angles between all rays and the optical axis of the HC enable the fulfillment of paraxial approximation conditions, thereby simplifying the calculation of light trajectories;[15,16] (3) the incident light, nearly parallel to the optical axis, facilitates uncomplicated optical alignment during the assembly process;[17] and (4) the overall cost is reduced without need of custom elements.

Nevertheless, HCs typically feature a cylindrical cell with mirrors placed at both ends. This configuration introduces several challenges during utilization. First, integrating a long cylindrical cell into a compact sensor is difficult. Second, achieving precise temperature control for a long cylindrical cell poses a significant challenge due to its dispersed mass. When an MPC is used outdoors, temperature variations can lead to thermal expansion or mechanical deformation of the MPC and also cause variation in the target gas line-strength. Therefore, precise temperature control is essential in applications requiring high precision and stability, such as carbon monitoring. Finally, mirrors of the HC have poor utilization efficiency due to their circular pattern, which results in inefficient use of mirror space.

In this Letter, we propose a calculation model of a rectangular-like HC (RLHC) to address the issues associated with traditional HCs. The theoretical design of the RLHC involves two key steps: (1) compressing the circular spot pattern on the two spherical mirrors of a

traditional HC into an ellipse to enhance mirror utilization efficiency, as shown in Fig. 1, and (2) introducing two-plane mirrors at the same inclined angle to fold the central axis line of the traditional HC, resulting in an RLHC, as illustrated in Fig. 2.

In Fig. 1(a), a traditional HC is shown consisting of two spherical mirrors (SM1 and SM2) with the same radius of curvature R, and the mirror spacing is d. We define the length of the long axis of an elliptical spot pattern as $2a$, the length of the short axis as $2b$, and the compressibility factor as τ ($\tau = a/b$). Using a 3D Cartesian coordinate system, the nth spot location on the two spherical mirrors is described by the coordinates (x_n, y_n) with the inclination angle of the ray (x_n', y_n'). According to the principle of the traditional HC, the coordinates (x_n, y_n) for the elliptical spot pattern are calculated as follows:[18]

$$\begin{aligned} x_n &= a\sin(n\theta+\alpha),\\ y_n &= b\sin(n\theta+\beta),\\ \tan\alpha &= \sqrt{\frac{2R}{d}-1}\Big/\left(1+R\frac{x_0'}{x_0}\right),\\ \tan\beta &= \sqrt{\frac{2R}{d}-1}\Big/\left(1+R\frac{y_0'}{y_0}\right),\\ d &= R(1-\cos\theta),\\ \theta &= (N-2)\pi/2N. \end{aligned} \tag{1}$$

Here, (x_0, y_0) and (x_0', y_0') are the initial location and inclination angle of the incident ray, respectively, N is the total number of reflections, and θ is half the angle of offset of the reflection point after each round trip.

To facilitate the calculation and implementation, we set the initial location (x_0, y_0) at $(0, -b)$ and let $\tan\alpha \times \tan\beta = -1$, which results in (x_0', y_0') being $(-\tau b\sqrt{(2R-d)/R^2 d},\ b/R)$. The nth spot location can be rewritten as

$$\begin{aligned} x_n &= \tau b\sin(n\theta),\\ y_n &= b\sin(n\theta), \end{aligned} \tag{2}$$

which is a standard elliptical spot pattern with the long axis coinciding with the x-axis and the short axis coinciding with the y-axis.

To create an RLHC, the optical path is folded m times by inserting two highly reflective plane mirrors, as shown in Fig. 2. The two plane mirrors are named PM1 and PM2 and are positioned at an i-degree angle to the y-axis and parallel to the x-axis, allowing for even folding of the optical path in the y-z plane. Assuming that the center of SM1 is the origin ($z_{SM1} = 0$ and $y_{SM1} = 0$) and ω represents the offset of the last folding point of the original optical axis on the left-hand side with respect to the z-axis, the centers of PM1, PM2, and SM2 (their z-coordinates and y-coordinates) can be expressed through geometric algebra as follows:

PM1:

$$z_{PM1} = \frac{d}{m+1} + \frac{2m-3+(-1)^{m+1}}{2\left[2m+1+(-1)^{m+1}\right]}\cdot\omega; \tag{3}$$

$$y_{PM1} = \frac{2m-3+(-1)^{m+1}}{2\left[2m+1+(-1)^{m+1}\right]}\cdot\frac{\omega}{\tan i}; \tag{4}$$

PM2:

$$z_{PM2} = \left[\frac{1}{2}+\frac{1+(-1)^m}{2m}\right]\cdot\omega; \tag{5}$$

$$y_{PM2} = \left[\frac{1}{2}+\frac{1+(-1)^m}{2m}\right]\cdot\frac{\omega}{\tan i}; \tag{6}$$

SM2:

$$z_{SM2} = \omega + \frac{d}{m+1}\cdot\frac{1+(-1)^m}{2}; \tag{7}$$

$$y_{SM2} = \frac{\omega}{\tan i}. \tag{8}$$

Here, ω can be expressed as

$$\omega = \frac{2m+1+(-1)^{m+1}}{2(m+1)}\cdot d\sin^2 i. \tag{9}$$

Note that when m is odd, SM2 is on the same side of SM1 in the y-z plane, as shown in Fig. 2(b); when the number of folding m is even,

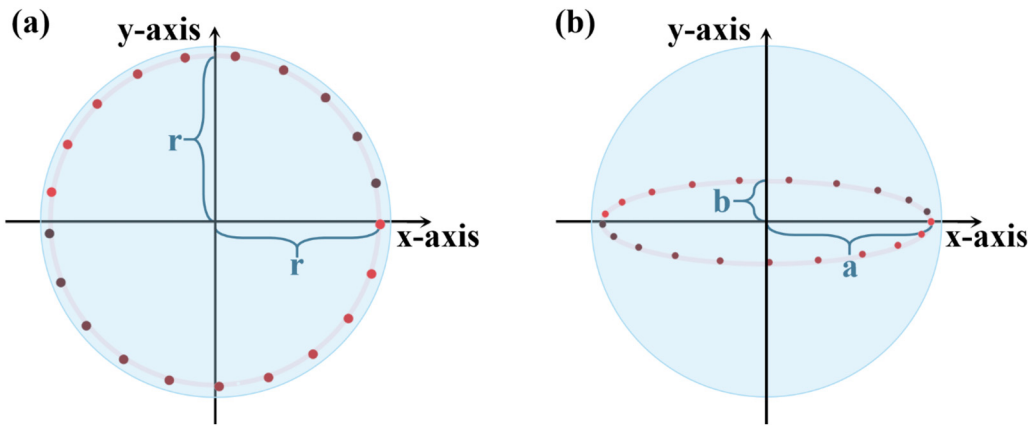

FIG. 1. (a) The spot pattern on the spherical mirror in HC is presented as a circle, taking the total number of reflections 41 as an example. (b) After compression, the spot pattern on the spherical mirror is presented as an ellipse, taking the total number of reflections 41 as an example. The compressibility factor is denoted as τ ($\tau = a/b$). As the number of reflections increases, the color of the spot gradually changes from dark red to bright red.

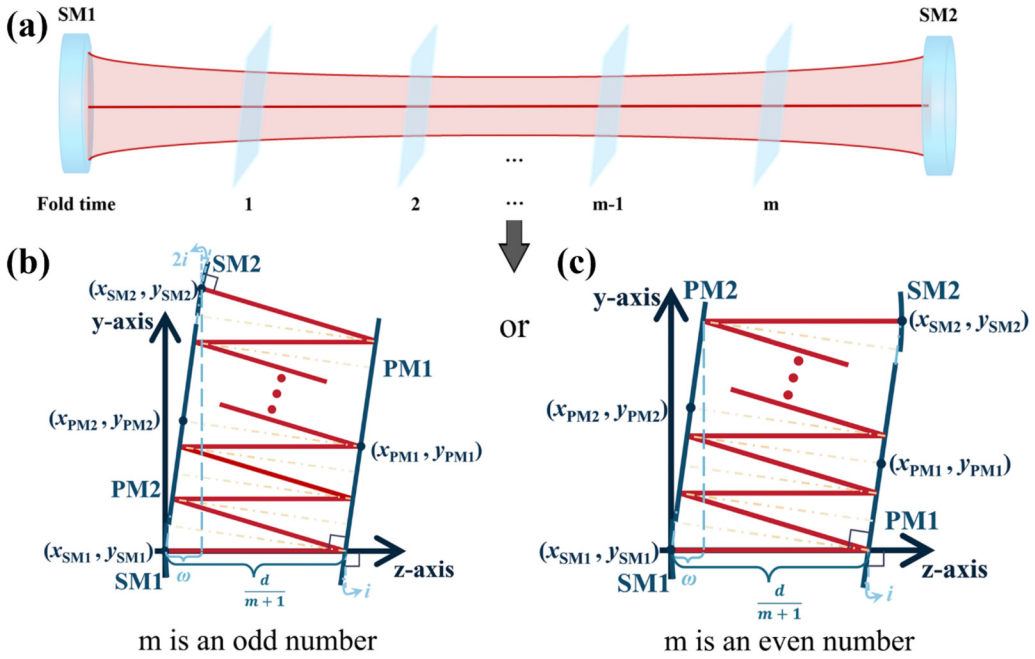

FIG. 2. Folding a traditional HC into an RLHC. (a) A traditional HC is evenly divided into m + 1 parts by m reflecting surfaces at the same angle. The thin red lines indicate the outer contours of all the rays of the traditional HC from the front view, and the bold red line indicates the central axis line of the traditional HC. (b) The traditional HC is sequentially folded by inserting two plane mirrors according to the reflecting surface, when the number of folding *m* is odd. (c) The traditional HC is sequentially folded by inserting two plane mirrors according to the reflecting surface, when the number of folding *m* is even.

SM2 is on the opposite side of SM1 in the y-z plane, as shown in Fig. 2(c). Furthermore, when m is 1, only PM1 is needed.

A small angle i may cause overlapping between the multiple elliptical spot patterns on the plane mirrors. To avoid overlapping, the angle i must satisfy

$$\frac{d}{m+1}\cdot \sin i > \frac{b}{\cos i}. \tag{10}$$

With increase in angle i, the distance between two elliptical spot patterns becomes larger, leading to wasted space on the plane mirror. A sparsity parameter η is introduced to indicate the density of these elliptical spot patterns on the plane mirrors, PM1 and PM2,

$$\eta = \frac{\frac{d\sin i}{m+1} - \frac{b}{\cos i}}{\frac{b}{\cos i}}. \tag{11}$$

A η value between 0 and 1 is appropriate for the utilization efficiency of these mirrors.

The volume and length of RLHC can be estimated as follows:

$$V \approx 2a^2 d\frac{(\eta+1)m+2}{\tau(m+1)}, \tag{12}$$

$$l \approx \frac{d}{m+1}. \tag{13}$$

The volume of RLHC is inversely proportional to the compressibility factor τ but positively related to the sparsity parameter η.

To obtain a square-like HC, let $d/(m+1) = \omega/\tan i$. The folding times can be calculated as follows:

$$m \approx \sqrt{\frac{d\tau}{(\eta+1)a}} - 1. \tag{14}$$

For a side-by-side comparison of the folding effect, two spherical mirrors with the same radius of curvature of 400 mm are utilized. The total number of reflections, N, is set to 41, resulting in a 369-mm mirror spacing, d, for the traditional HC and a total optical path length of 15.5 m. For RLHC, two parallel inclined plane mirrors are added to fold the tradition HC. In the x-y plane, the initial location (0, −3) of the incident ray is selected, leading to an inclination angle (−0.0324, 0.0075) of the incident ray. The compressibility factor, τ, and the sparsity parameter, η, are fixed to be 4 and 0.224, respectively. Hence, the inclination angles of the plane mirrors can be calculated according to Eq. (11). Comparison of the folding effect between the traditional HC and the RLHCs with 1–8-times folding is carried out. The results are presented in Table I in terms of the cell length, l (mm), tilt angle of the

TABLE I. Length, *l* (mm), volume, *V* (ml), and total number, N, of reflections of RLHC and insertion angle, *i*(degree), of the plane mirror in the y-z plane for different folding times.

Folding times	0	1	2	3	4	5	6	7	8
l (mm)	369	185	123	92	74	62	53	46	41
i (°)	⋯	1.14	1.71	2.28	2.85	3.43	4	4.58	5.16
V (ml)	167	57.2	52.6	50.3	48.9	48.0	47.3	46.8	46.5
N	41	83	125	167	209	251	293	335	377

plane mirrors, i (degree), cell volume, V (ml), and total number of reflections, N. With increase in the number of folding, the cell length becomes shorter. The traditional HC is compressed from a cylindrical cell to an RLHC. Moreover, the RLHC has a small volume of ∼50 ml, which is ∼3 times smaller than that of the traditional HC. This reduced volume is primary attributed to the contribution of the elliptical spot pattern, providing high utilization efficiency of the mirror surface. With 8 times folding, an effective optical path of 15.5 m can be realized in a square-like HC with a length of 4.4 cm and a volume of 46.5 ml.

A silver-coated spherical mirror typically exhibits a reflectance of >97%. As the number of reflections increases, the light loss gradually becomes more substantial. For instance, an incident beam with an initial power of 10 mW, after 200 reflections, retains a power of 23 μW. After 350 reflections, it diminishes to only 0.2 μW, and after 400 reflections, it drops to just 51 nW. Therefore, an RLHC with folding times of 6 and 7 is deemed reasonable and achievable when employing silver-coated spherical mirrors. To validate the calculation mode, the two RLHCs with folding times of 6 and 7 in Table I are simulated using TracePro. The size of the incident hole on SM1 is set to 1.5 mm. Consistent with the unfolded original HC, the light exits through the incidence hole after all reflections have been completed. The results are illustrated in Fig. 3. The 3D model of the 6- and 7-times folding RLHC are shown in Figs. 3(a) and 3(d), respectively. The spot patterns on SM1and PM2 for 6-times folding and on SM1, PM2, and SM2 for 7-times folding are depicted in Figs. 3(b) and 3(e), respectively. The spot patterns on PM1 and SM2 for 6-times folding and on PM1 for 7-times folding are presented in Figs. 3(c) and 3(f), respectively. It can be observed that the elliptical spot pattern on the spherical mirrors, SM1 and SM2, is larger than that on the plane mirrors, PM1 and PM2. This discrepancy arises because, in a traditional HC, the size of the ellipse in which the spot is located within an arbitrary x-y interface in free space is smaller than on the two spherical mirrors, as shown in Fig. 2(a).

The simulation results effectively demonstrate that a traditional HC can be folded into an RLHC according to the calculation model proposed in this Letter. Furthermore, three advantages are realized in the folding scheme: (1) The length of the traditional HC is significantly reduced, with the original 369 mm mirror spacing being reduced to 53 and 46 mm for 6- and 7-times folding, respectively. (2) The volume is significantly compressed with the original 167 ml being reduced into 47.3 and 46.8 ml for 6- and 7-times folding, respectively. (3) A cylindrical cell is transformed into a RLHC, facilitating temperature control and enabling the creation of a compact sensor.

Two silver-coated spherical mirrors, each with a reflectance of 97%, are employed to experimentally realize the 6-times folding RLHC, as illustrated in Fig. 4. All parameters maintain consistency with those employed in the TracePro simulation. The parameters and arrangement depicted in Fig. 4(a) are identical to those in Fig. 3(a). In Fig. 4(b), the cell length along the z-axis measured 53 mm, aligning with the parameters detailed in Table I. The spot patterns observed in Figs. 4(c) and 4(d) exhibit excellent agreement with those in Figs. 3(b) and 3(c), thereby affirming the rationality and feasibility of the calculation model for a rectangular-like Herriott cell based on the folded-optics method.

In conclusion, we developed a calculation model for the RLHC, incorporating two parallel plane mirrors as reflector at a specific angle. The use of plane mirrors avoids introducing spherical aberration and

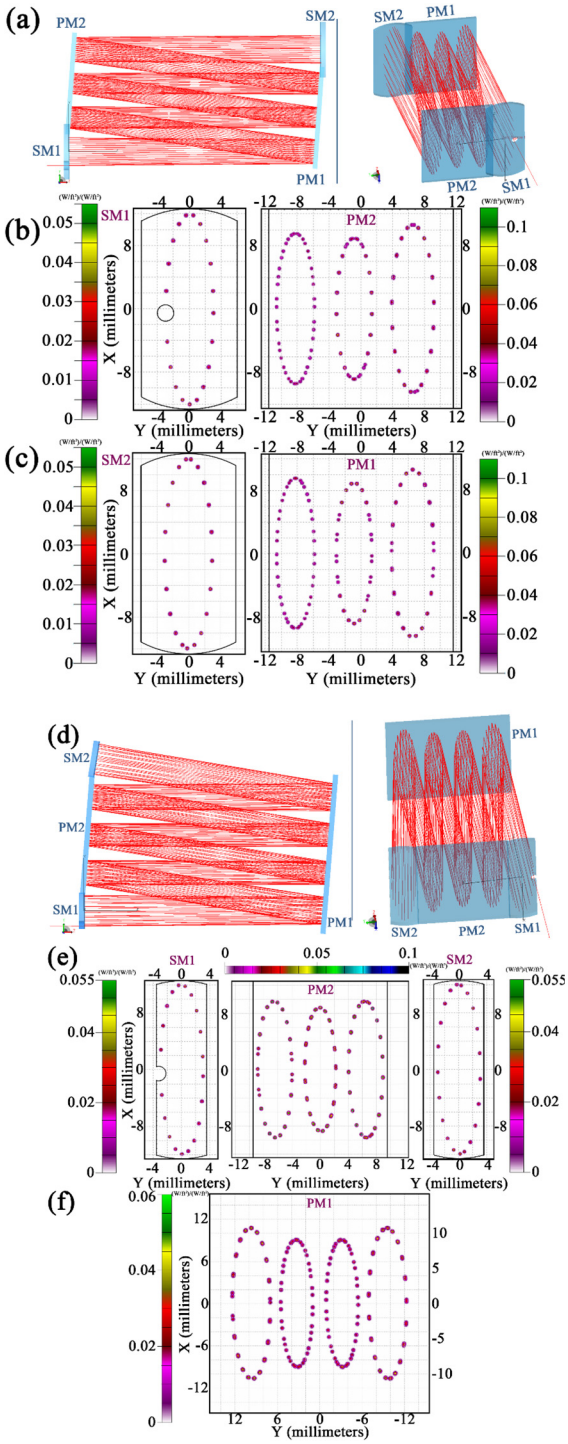

FIG. 3. Simulation plots for 6-times and 7-times folding, respectively. (a) and (d) 3D models of the 6-times and 7-times folding RLHCs by using TracePro. (b), (c), (e), and (f) The spot patterns on SM1, PM1, PM2, and SM2 when simulated for 6-times and 7-times folded RLHCs, respectively, using TracePro. The light spot patterns on panels (b), (c), (e), and (f) are the patterns of light spots seen when facing the emitting side of the mirror, respectively.

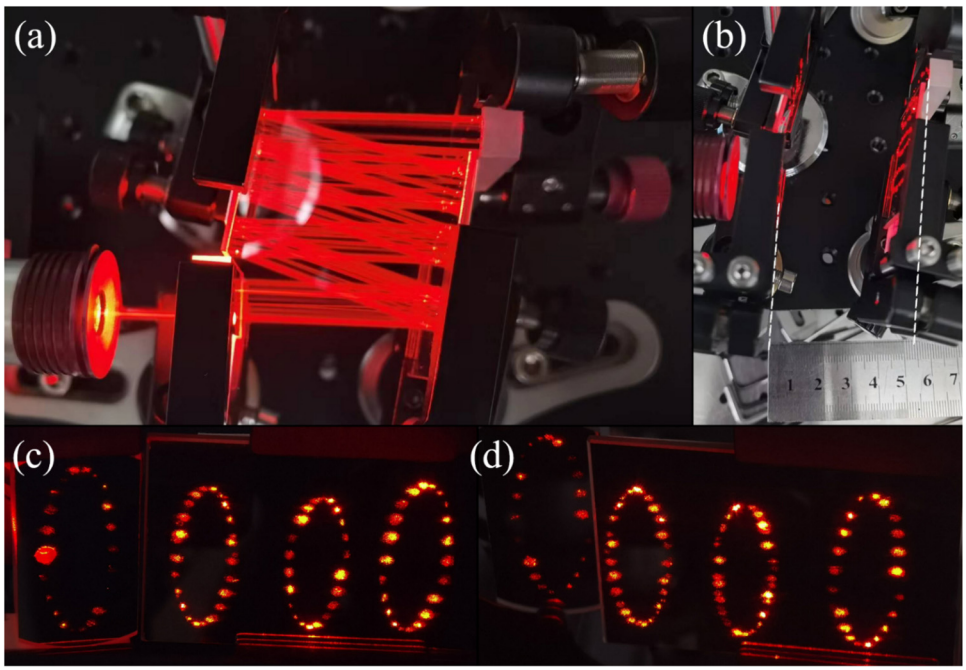

FIG. 4. Optical trajectories and spot patterns in a 6-times folding RLHC. (a) Top view of the optical trajectory in the 6-times folding RLHC. (b) RLHC length. (c) Spot patterns on SM1 and PM2 when facing the right-side mirror. (d) Spot patterns on SM2 and PM1 when facing the left-side mirror.

maintains the paraxial approximation of the traditional HC. Therefore, the RLHC preserves the same light beam shape as the traditional HC. The folded-optics approach effectively reduces the length and volume of conventional HCs, paving the way for a sensitive, cost-effective, and compact trace gas sensor suitable for large-scale deployment in distributed sensor networks and handheld mobile devices. Further topics of interest include designing the mechanical structure, evaluating the performance of the RLHC for trace gas sensing, and developing trace gas sensors based on this configuration.

This project is sponsored by the National Natural Science Foundation of China (NSFC) (Nos. 62235010, 62175137, 62122045, and 62075119), the Shanxi Science Fund for Distinguished Young Scholars (No. 20210302121003), and the Shanxi Provincial Special Fund for Scientific and Technological Cooperation and Exchange (202304041101019).

AUTHOR DECLARATIONS

Conflict of Interest

The authors have no conflicts to disclose.

Author Contributions

Qingyuan Tian, Ruyue Cui, and Lei Dong contributed equally to this work

Qingyuan Tian: Conceptualization (equal); Data curation (equal); Formal analysis (equal); Funding acquisition (equal); Investigation (equal); Methodology (equal); Project administration (equal); Resources (equal); Software (equal); Supervision (equal); Validation (equal); Visualization (equal); Writing – original draft (equal); Writing – review & editing (equal). **Hongpeng Wu:** Funding acquisition (equal); Investigation (equal); Methodology (equal). **Ruyue Cui:** Conceptualization (equal); Data curation (equal); Formal analysis (equal); Funding acquisition (equal); Investigation (equal); Methodology (equal); Project administration (equal); Resources (equal); Software (equal); Supervision (equal); Validation (equal); Visualization (equal). **Yongyong Hu:** Conceptualization (equal); Methodology (equal); Software (equal). **Yan Xue:** Conceptualization (equal); Data curation (equal); Visualization (equal). **Gang Wang:** Methodology (equal); Visualization (equal). **Jiapeng Wang:** Methodology (equal); Software (equal); Visualization (equal). **Yong Wang:** Methodology (equal); Visualization (equal). **Xiaoli Liu:** Resources (equal); Visualization (equal). **Frank K. Tittel:** Conceptualization (equal); Funding acquisition (equal); Investigation (equal); Resources (equal). **Lei Dong:** Conceptualization (equal); Data curation (equal); Formal analysis (equal); Funding acquisition (equal); Investigation (equal); Methodology (equal); Project administration (equal); Resources (equal); Validation (equal); Writing – review & editing (equal).

DATA AVAILABILITY

The data that support the findings of this study are available from the corresponding author upon reasonable request.

REFERENCES

[1]L. Dong, F. K. Tittel, C. G. Li, N. P. Sanchez, H. P. Wu, C. T. Zheng, Y. J. Yu, A. Sampaolo, and R. J. Griffin, Opt. Express **24**, A528–A535 (2016).
[2]M. Gu, J. Chen, J. Mei, T. Tan, G. Wang, K. Liu, G. Liu, and X. Gao, Opt. Express **30**, 43961–43972 (2022).
[3]S. D. Qiao, A. Sampaolo, P. Patimisco, V. Spagnolo, and Y. F. Ma, Photoacoustics **27**, 100381 (2022).
[4]R. Y. Cui, H. P. Wu, F. K. Tittel, V. Spagnolo, W. D. Chen, and L. Dong, Photoacoustics **35**, 100580 (2023).
[5]Y. F. Ma, T. T. Liang, S. D. Qiao, X. N. Liu, and Z. T. Lang, Ultrafast Sci. **3**, 0024 (2023).

[6]S. Ozharar and A. Sennaroglu, Opt. Lett. **42**, 1935–1938 (2017).
[7]J. J. Chen, G. S. Wang, K. Liu, T. Tan, G. Cheng, X. Tian, and X. M. Gao, Spectrosc. Spectral Anal. **39**, 292–296 (2019).
[8]Y. N. Cao, G. Cheng, X. Tian, G. S. Wang, Y. Cao, C. Y. Sun, Y. L. Zhang, G. X. Cheng, and H. T. Yang, Optik **227**, 166095 (2021).
[9]R. Y. Cui, L. Dong, H. P. Wu, S. Z. Li, X. K. Yin, and F. K. Tittel, Opt. Lett. **44**, 1108 (2019).
[10]A. Hudzikowski, A. Głuszek, K. Krzempek, and J. Sotor, Opt. Express **29**, 26127 (2021).
[11]G. Cheng, Y.-N. Cao, X. Tian, J.-J. Chen, and J.-J. Wang, Front. Phys. **10**, 907715 (2022).
[12]M. J. Wang, D. Wang, Y. Lv, P. Y. Li, D. Li, and Y. S. Li, Infrared Phys. Technol. **116**, 103811 (2021).
[13]T. T. Liang, S. D. Qiao, X. N. Liu, and Y. F. Ma, Chemosensors **10**, 321 (2022).
[14]R. Y. Cui, L. Dong, H. P. Wu, S. Z. Li, L. Zhang, W. G. Ma, W. B. Yin, L. T. Xiao, S. T. Jia, and F. K. Tittel, Opt. Express **26**, 24318 (2018).
[15]B. Fang, W. X. Zhao, N. N. Yang, C. H. Wang, H. Zhou, and W. J. Zhang, Chin. J. Quantum Electron. **38**, 617 (2021).
[16]R. Y. Cui, L. Dong, H. P. Wu, W. G. Ma, L. T. Xiao, S. T. Jia, W. D. Chen, and F. K. Tittel, Anal. Chem. **92**, 13034–13041 (2020).
[17]L. Y. Hao, G. R. Wu, Q. Shi, Q. Li, H. Lin, and Q. S. Zhu, Chin. J. Chem. Phys. **14**, 147–153 (2001).
[18]D. Herriott, H. Kogelnik, and R. Kompfner, Appl. Opt. **3**, 523–526 (1964).